



A novel myocardium segmentation approach based on neutrosophic active contour model

Yanhui Guo^{a,*}, Guo-Qing Du^b, Jing-Yi Xue^c, Rong Xia^d, Yu-hang Wang^b

^a Department of Computer Science, University of Illinois at Springfield, Springfield, IL USA

^b Department of Ultrasound, Second Affiliated Hospital of Harbin Medical University, Harbin, China

^c Department of Cardiology, First Affiliated Hospital of Harbin Medical University, Harbin, China

^d Oracle Corporation, Westminster, CO, USA



ARTICLE INFO

Article history:

Received 24 March 2016

Revised 9 February 2017

Accepted 15 February 2017

Keywords:

Myocardial contrast echocardiography (MCE)

Myocardium detection

Neutrosophic similarity

Active contour model

ABSTRACT

Background and objectives: Automatic delineation of the myocardium in echocardiography can assist radiologists to diagnosis heart problems. However, it is still challenging to distinguish myocardium from other tissue due to a low signal-to-noise ratio, low contrast, vague boundary, and speckle noise. The purpose of this study is to automatically detect myocardium region in left ventricle myocardial contrast echocardiography (LVMCE) images to help radiologists' diagnosis and further measurement on infarction size.

Methods: The LVMCE image is firstly mapped into neutrosophic similarity (NS) domain using the intensity and homogeneity features. Then, a neutrosophic active contour model (NACM) is proposed and the energy function is defined by the NS values. Finally, the ventricle is detected using the curve evolving results. The ventricle's boundary is identified as the endocardium. To speed up the evolution procedure and increase the detection accuracy, a clustering algorithm is employed to obtain the initial ventricle region. The curve evolution procedure in NACM is utilized again to obtain the epicardium, where the initial contour uses the detected endocardium and the anatomy knowledge on the thickness of the myocardium.

Results: Echocardiographic studies are performed on 10 male Sprague-Dawley rats using a Vivid 7 system including 5 normal cases and 5 rats with myocardial infarction. The myocardium boundaries manually outlined by an experienced radiologist are used as the reference standard for the performance evaluation. Two metrics, Hdist and AvgDist, are employed to evaluate the detection results. The NACM method was compared with those from the eliminated particle swarm optimization (EPSO) and active contour model without edges (ACMWE) methods. The mean and standard deviation of the Hdist and AvgDist on endocardium are 6.83 ± 1.12 mm and 0.79 ± 0.28 mm using EPSO method, 7.12 ± 0.98 mm and 0.82 ± 0.32 mm using ACMWE method, and 4.55 ± 0.9 mm and 0.58 ± 0.18 mm using NACM method, respectively. The improvement on epicardium is much more significant, and two metrics are decreased from 7.45 ± 1.24 mm, and 1.47 ± 0.34 mm using EPSO method, and 8.21 ± 0.43 mm, and 1.73 ± 0.47 mm using ACMWE method, to 4.94 ± 0.82 mm, and 0.84 ± 0.22 mm using NACM method, respectively.

Conclusions: The proposed method can automatically detect myocardium accurately, and is helpful for clinical therapeutics to measure myocardial perfusion and infarct size.

© 2017 Elsevier B.V. All rights reserved.

1. Introduction

Myocardial infarction (MI) is one of serious heart diseases, and the infarcted area can lead to the subsequent death of cardiomyocytes and vascular cells in the border area. The key point to reduce the mortality associated with MI is to limit and reduce infarct size [1]. Therefore, detecting myocardium and assessing infarction

size are critical in the study of morphology and function of myocardium [2].

Automatic delineation of the myocardium in echocardiography is used to aid the diagnosis of heart problems, such as ischaemia, by enabling quantification of wall thickening and wall motion abnormalities. Distinguishing between myocardial and non-myocardial tissue is, however, difficult due to a low signal-to-noise ratio, low contrast, vague boundary, speckle noise and other indeterminacy information.

Myocardial contrast echocardiography (MCE) is a non-invasive diagnostic technique providing information of cardiac function and

* Corresponding author.

E-mail address: yguo56@uis.edu (Y. Guo).

hemodynamics. This has been used to obtain information of both MI and myocardial ischemia for the diagnosis purpose [3–5]. However, most methods based on MCE have relied on manual visual analysis, leading to errors of operator subjectivity; the accuracy of manual analysis in detecting on myocardium borders depends on the investigators' experience and their ability to distinguish artifacts from actual perfusion defects. It is evident that accurate and automatic detection of myocardium on MCE is a critical and valuable step and few studies have addressed the problem [6–8].

Computer aided diagnosis (CAD) system has been developed to identify the infarcted myocardium [9]. Many approaches have been proposed to identify and track myocardial borders [10], the ventricular cavity (i.e. endocardium) [11], epicardial boundary [12], and the full myocardium using echocardiographic images [13,14].

Ziwirn et al. [8] presented an endocardial boundary (inner boundary) detection method in myocardial images characterized by low signal-to-noise ratios. It converted the frames in Cartesian coordinates into polar coordinates, and applied a set of filters in order to compute the initial estimation of the endocardial boundary. The final estimation of the endocardial boundary was produced by an error correction process using both spatial and temporal filtering. The estimated boundaries are converted into Cartesian coordinates, for display. However, it is not a fully automatic approach and it needs manually defined reference points. Zhang et al. [10] presented a method to globally affine register a real time 3-D ultrasound volume to a 2-D cardiovascular MR image. The local phase presentation of both images was utilized as an image descriptor of "featureness". Phasemutual information was employed as the similarity metric. The registration process was built in a multi-scale frame-work to estimate the global affine transformation using a differential technique. However, its accuracy depends on the registration process which is time consuming. Sigit et al. [11] used collinear and triangle equation algorithms to detect and reconstruct the boundary of the cardiac cavity. It employed high boost filter to enhance the high frequency component and the morphological and thresholding operators to eliminate noise and convert the image into a binary image. Finally, the collinear and triangle equations are used to detect and reconstruct the more precise cavity boundary. Seng et al. [12] proposed an automated left ventricle detection method for two-dimensional echocardiographic images that could serve as an initialization for deformable models. The proposed approach consists of pre-processing and post-processing stages. The pre-processing stage enhances the overall contrast and reduces speckle noise, whereas the post-processing enhances the segmented region and avoids the papillary muscles. It only provides an initial contour of the left ventricle. Dietenbeck et al. [15] proposed a method to segment the whole myocardium in 2D echographic images. A level set model constrained by a shape formulation allowed to model both contours of myocardium. It can segment the whole myocardium for the four main views used in clinical routine. Dietenbeck et al. [14] extended a level-set method to track the whole myocardium in echocardiographic sequences. It enforced temporal coherence by adding a new motion prior energy to the existing framework, which was expressed as new constraint that enforces the conservation of the levels of the implicit function along the image sequence. However, it needs multiple views to finish the detection.

In different CAD approaches, myocardium segmentation and detection is a crucial step whose performance further analysis on functional measures of myocardium and fraction size. Lynch et al. [16] presented a level-set segmentation of the myocardium of the left ventricle of the heart by using a priori information in magnetic resonance imaging (MRI). Two fronts representing the endocardium and epicardium boundaries of the left ventricle were evolved as the zero level-set of a higher dimension function. A stopping term was introduced using both gradient and

region-based information. Wong et al. [17] proposed a velocity-constrained front propagation approach for myocardium segmentation from magnetic resonance intensity image (MRI) and its matching phase contrast velocity (PCV) images. The curve evolution criterion was defined on the prior probability distribution of the myocardial boundary and the conditional boundary probability distribution, which was constructed from the MRI intensity gradient, the PCV magnitude, and the local phase coherence of the PCV direction. For the first image frame, a gradient marching level set step was used to approach the boundary, and a narrowband was formed around the curve. The initial boundary was then refined using the full information from priors and all three image sources. For the other frames, the resulting contours from the previous frames were used as initialization contours, and refinement steps were taken. However, the curve evolution criterion depends on the prior probability which is related to the training dataset. Li et al. [18] presented a semi-automated segmentation method for short-axis cardiac CT and MR images. It used two different energy functions for endocardium and epicardium segmentation to account for their distinctive characteristics, proposed a dual-background model for representing intensity distributions of the background in epicardium segmentation, designed a shape prior term, and estimated myocardium thickness using edge information. Lynch et al. [19] developed a segmentation approach to extract the epicardium and endocardium boundaries of the left ventricle using multi-slice and multi-phase MRI images of the heart. The images were segmented using a diffusion-based filter followed by an unsupervised clustering technique, and the resulting labels were checked to locate the cavity on left ventricle. The wall between these two blood-pools was measured to give an approximate thickness for the myocardium, and then it was used to find appropriate segments of the epicardium boundary. However, selection of the clustering number is a challenging problem.

A stochastic deformable model was proposed for the segmentation of the myocardium in MRI [20]. The segmentation was posed as a probabilistic optimization problem in which the optimal time-dependent surface was obtained for the myocardium of the heart in a discrete space of locations built upon simple geometric assumptions. The segmentation solution was obtained by the maximization of the posterior marginal for the myocardium location in a Markov random field framework which optimally integrated temporal-spatial smoothness with intensity and gradient related features in an unsupervised way by the maximum likelihood estimation of the parameters of the field. Lempitsky et al. [21] treated the segmentation problem as a two-class 3D patch classification task, solving it using random forests to obtain delineations of myocardium. However, this method is sensitive to noise which often occurs in medical images. Recently, machine learning methods such as random forest have been used to segment the myocardium in MCE [22]. It used a statistical shape model of the myocardium to guide the random forest segmentation. Lempitsky et al. [23] employed random forest classification for delineation of myocardium. It treated the segmentation problem of myocardial and non-myocardial tissue as a two-class classification task.

Although these methods are useful, most of them are semi-automatic segmentation algorithm and applicable to traditional ultrasound images and do not work well on the MCE image due to its own characteristics. Therefore, it still remains a challenge for CAD systems to properly and automatically segment and detect myocardium on MCE images. MCE images retain some properties that cause indeterminacy: i.e. vague boundaries, high amount of speckles, low contrast between suspicious areas and tissues. Therefore, dealing with the indeterminacy is necessary to improve the quality of images analysis on MCE. In this paper, we propose a novel CAD approach for fully automatic myocardium segmentation on MCE image based on neutrosophic similarity measurement and

active contour model. The short-axis left ventricle MCE (SLVMCE) image is interpreted by neutrosophic set (NS) and the similarity value is defined using intensity and homogeneity of the SLVMCE image in NS which has advantages to interpret the indeterminant information on MCE such as vague boundary, low contrast and speckle noise. Then, a neutrosophic active contour model (NACM) is proposed and energy functions in NACM are defined using the neutrosophic similarity values (NSV). The myocardium region is finally detected by using the curve evolve results.

The remainder of the paper is structured as follows: **Section 2** depicts the proposed method and introduces the neutrosophic active contour method. **Section 3** discusses the experiment and comparison results, and conclusions are brought in **Section 4**.

2. Proposed method

This paper proposes a novel neutrosophic active contour model (NACM) to segment and detect the myocardium region in the short-axis left ventricle of myocardial contrast echocardiogram (SLVMCE) image. At first, the SLVMCE image is transformed into a neutrosophic set domain, and the similarity value is defined using intensity and homogeneity of the SLVMCE image. Then, energy functions in active contour model are defined based on the neutrosophic similarity value (NSV). Finally, the inner and outer boundaries of myocardium are identified by using the curve evolve results.

2.1. Neutrosophic similarity value

SLVMCE is a type of ultrasound image and has some indeterminacy information such as speckle noise, vague edge, and low contrast. Neutrosophic set (NS) has an advantage to describe the indeterminacy information on image, and in NS theory, a member of a set has a degree of truth, a falsity degree and an indeterminacy degree [24]. It has been successfully applied into image segmentation for noisy images [25–28].

In this section, NS is used to depict the indeterminacy information on SLVMCE, and neutrosophic similarity value (NSV) is defined using intensity and homogeneity information to remove the indeterminacy information.

First, the SLVMCE image is transformed into NS domain using intensity values and homogeneity values as follows:

$$T_g(x, y) = \frac{g(x, y) - g_{\min}}{g_{\max} - g_{\min}} \quad (1)$$

$$I_g(x, y) = \frac{Dg(x, y) - Dg_{\min}}{Dg_{\max} - Dg_{\min}} \quad (2)$$

where T_g and I_g are the true and indeterminate membership values in neutrosophic set under intensity condition, respectively. g_{\min} and g_{\max} are minimum and maximum of the intensity, and Dg_{\min} and Dg_{\max} are minimum and maximum of the gradient value of intensity, respectively.

$$T_h(x, y) = \frac{hm(x, y) - hm_{\min}}{hm_{\max} - hm_{\min}} \quad (3)$$

$$I_h(x, y) = \frac{Dh(x, y) - Dh_{\min}}{Dh_{\max} - Dh_{\min}} \quad (4)$$

$$hm(x, y) = TEM(g(x, y)) \quad (5)$$

$$Dh(x, y) = |Gd_h(x, y)| \quad (6)$$

where T_h and I_h are the true and indeterminate membership values in neutrosophic set under homogeneity domain, respectively. hm is the homogeneity value and defined as the filtered result using the

texture energy measures (TEM) filters [29]. Dh is the magnitude value of gradient on homogeneity. Dh_{\min} and Dh_{\max} are minimum and maximum of the gradient value of homogeneity, respectively.

The similarity value is defined using the neutrosophic values from intensity and homogeneity information.

$$S(x, y) = \frac{w_1 T_g(x, y) (1 - I_g(x, y))}{\sqrt{T_g^2(x, y) + I_g^2(x, y)}} + \frac{w_2 T_h(x, y) (1 - I_h(x, y))}{\sqrt{T_h^2(x, y) + I_h^2(x, y)}} \quad (7)$$

where w_1 and w_2 are weight for two neutrosophic values. In our experiment, $w_1=0.4$ and $w_2=0.6$ which are obtained by trial and error way.

2.2. Neutrosophic active contour model

Contour might be a boundary of objects in an image. The active contour model (ACM) (also called snake) is an energy minimizing, deformable spline which is influenced by constraint and image forces that pull it towards object contours and internal forces that resist deformation. ACM, in particular, is designed to solve problems where the approximate shape of the boundary is known.

In the traditional ACM algorithm, the energy function is defined as [30]:

$$E_s^* = \int_0^1 \left(\alpha \left| \frac{\partial}{\partial s} \bar{v} \right|^2 + \beta \left| \frac{\partial^2}{\partial s^2} \bar{v} \right|^2 + E_{ext}(v(s)) \right) ds \quad (8)$$

$$E_{ext} = -|\nabla I(s)|^2 \quad (9)$$

where α and β are user-defined weights, and they control the internal energy function's sensitivity to the amount of stretch and the amount of curvature, respectively. $\nabla I(s)$ is the gradient of the image I at point s . In the proposed neutrosophic active contour model (NACM), the image I is replaced by the neutrosophic similarity value S and the energy function is redefined as:

$$E_{NACM}^* = \int_0^1 \left(\alpha \left| \frac{\partial}{\partial s} \bar{v} \right|^2 + \beta \left| \frac{\partial^2}{\partial s^2} \bar{v} \right|^2 - |\nabla S(s)|^2 \right) ds \quad (10)$$

The initial contour is an important parameter for curve evolution in ACM, which will determine the final result and evolution speed. In the NACM method for myocardium detection, an unsupervised clustering algorithm, k-means clustering is employed on the NSV image to determine the belonging of each pixel on SLVMCE image. The NSV image is clustered into three categories. Because neutrosophic similarity value has a good ability to describe the indeterminant information such as noise, vague edge, and low contrast in images, the clustering algorithm is able to separate the ventricle and myocardium regions with better performance [31–35].

The clustered region with high value of group center value is used as the initial ventricle region based on the characteristic of SLVMCE and its boundary as the initial contour for NACM.

2.3. Myocardium detection

In NACM method, contour of ventricle evolves on the NSV image and its energy functions are updated using the values on NSV iteratively. After termination criterion is satisfied, the accurate boundary is found on the ventricle region which is used as the boundary of endocardium.

In MCE image of short-axis left ventricle, the epicardium has a similar shape as endocardium. According to this anatomy information, the initial epicardium region is obtained by using a morphology dilation operation on the endocardium. The size of the element structure in dilation operation is determined by the knowledge of the anatomy of myocardium's thickness, which is estimated adaptively using the distance between the endocardium and diaphragm.

It is not accurate enough to have the epicardium only by dilated endocardium boundary, especially for the myocardium with perfusion or infarction. In order to make the result more accurate, the NACM method is taken again on the NSV image of SLVMCE to polish the epicardium boundary in which the initial contour is the dilated endocardium. Finally, the outlines of the ventricle and myocardium are identified as the endocardium and epicardium, respectively.

The entire steps can be summarized as follows:

1. Transform SLVMCE image into a neutrosophic domain;
2. Compute neturosophic similarity value of the SLVMCE image to obtain NSV image;
3. Take clustering algorithm on NSV image and have the region with highest center value as the initial contour of the vertical region;
4. Define the energy function in NACM using the values in NSV and the contour evolution result is used as the inner boundary of myocardium;
5. Run the NACM again to obtain the outer boundary of myocardium whose initial contour is the dilated result on the inner boundary of myocardium;
6. Identify the myocardium region based on the inner and outer boundary.

2.4. Evaluation metrics

The myocardium boundaries manually outlined by an experienced radiologist were used as the reference standard for performance evaluation of the myocardium detection method. To evaluate the detection results quantitatively, two metrics were employed to compare the segmentation results with the experienced radiologists' manual segmentation results.

Let $C = \{c_1, c_2, \dots, c_p\}$ be the computer-identified boundary that contains p singly-connected points, and $R = \{r_1, r_2, \dots, r_q\}$ be the radiologist's manually outlined boundary that contains q singly-connected points. The Euclidean distance between a computer-identified boundary point c_i and a reference standard point r_j is $\text{Dist}(c_i, r_j)$, or equivalently, $\text{Dist}(r_j, c_i)$. The accuracy of myocardium detection is evaluated by two performance metrics on edoncardium and epicardium.

(1) Hausdorff distance between the boundaries C and R ($H\text{dist}$)

$$\begin{aligned} H\text{dist} &= \max \left\{ \max_{c_i \in C} \left\{ \min_{r_j \in R} \{\text{Dist}(c_i, r_j)\} \right\}, \right. \\ &\quad \left. \max_{r_j \in R} \left\{ \min_{c_i \in C} \{\text{Dist}(r_j, c_i)\} \right\} \right\} \end{aligned} \quad (11)$$

(2) Average distance between the boundaries C and R (AvgDist)

$$\begin{aligned} \text{AvgDist} &= \frac{1}{2} \left(\frac{1}{p} \sum_{i=1}^p \min_{r_j \in R} \{\text{Dist}(c_i, r_j)\} \right. \\ &\quad \left. + \frac{1}{q} \sum_{j=1}^q \min_{c_i \in C} \{\text{Dist}(r_j, c_i)\} \right) \end{aligned} \quad (12)$$

The distance measures are calculated in units of mm.

3. Experimental results and discussions

3.1. Materials

In this experiment, 10 adult male Sprague-Dawley (SD) rats (280–300 g) were obtained from the Animal Central facility of the

Second Affiliated Hospital of Harbin Medical University, China, including 5 normal cases and 5 cases with myocardial infarction. Animal procedures were approved by the University's Committee for the Care of Experimental Animals.

Echocardiographic studies were performed using a Vivid 7 system (GE Healthcare, Milwaukee, WI, USA) equipped with a 10S transducer (8–12 MHz). The styrofoam board was tilted to maintain the rat in the left lateral decubitus position during image acquisition. The contrast agent was the commercially available sulphur hexafluoride phospholipid-encapsulated microbubble SonoVue (Bracco Medical Inc., Italy). The MCE images were acquired after peak myocardial opacification, until the disappearance of contrast from the myocardium. Contrast-enhanced images were obtained in left ventricle short-axis view (mitral valve, papillary muscle and apical levels) and image data was recorded on magneto-optical disks for offline analysis.

3.2. Experimental results

The original SLVMCE image (Fig. 1a) was first mapped into neutrosophic similarity value shown in Fig. 1b, in which indeterminate information is suppressed while preserving boundary features and the contrast between the left ventricle region and background is greatly enhanced. The gray scale images were clustered into label images, facilitating the detection of the ventricle region (Fig. 1c). After NACM segmentation on NSV image, the endocardial contour was marked using a red line and the epicardial border was marked by a blue line (Fig. 1d.) From the final results, it is demonstrated that the NACM method could extract ventricle region while closely, precisely, and clearly conforming to myocardium contours.

4. Discussions

There is an inherent difficulty in visually identifying regional differences in myocardial perfusion from a series of frames [36]. MCE can be used to identify non-perfused regions and detect infarcted myocardium [37,38]. However, these process is usually taken by visual inspection on an echocardiographic image, and using MCE to assess regional perfusion or viability has relied on subjective interpretations of MCE images [36,39]. Previous studies have suggested that automatic detection for the myocardial perfusion of all the segments can efficiently eliminate the visual differences using the aforementioned CAD system [40,41].

In the experimental results, the NACM algorithm is a better way for segmenting SLVMCE images and they are very close to the reference standard on visual. Proper segmentation of the myocardium is essential, as it is absolutely required for future analysis of myocardial perfusion.

During the detection, the SLVMCE images became uniform and facilitated automated segmentation after mapping into the NSV domain. In addition, the curve evolution in NACM can identify the boundaries of endocardium and epicardium with high accuracy. Figs. 2 and 3 demonstrate the detection results on two cases with different cardiac cycles. The NACM results are also compared with the manual results by an experienced radiologist. The myocardium boundaries manually outlined by an experienced radiologist are used as the reference standard. Several examples are listed in Fig. 2 to demonstrate the comparison between computer detection results with manual results, in which the computer detected results are marked in red and reference standards are in blue line. In addition, the indeterminate information of the image is identified using arrow marks.

A total of 182 images were selected from our dataset and the boundaries were manually outlined and used as the reference standard for performance evaluation. In comparison with the radiologist's manual outlines, the performance metrics ($H\text{dist}$ and

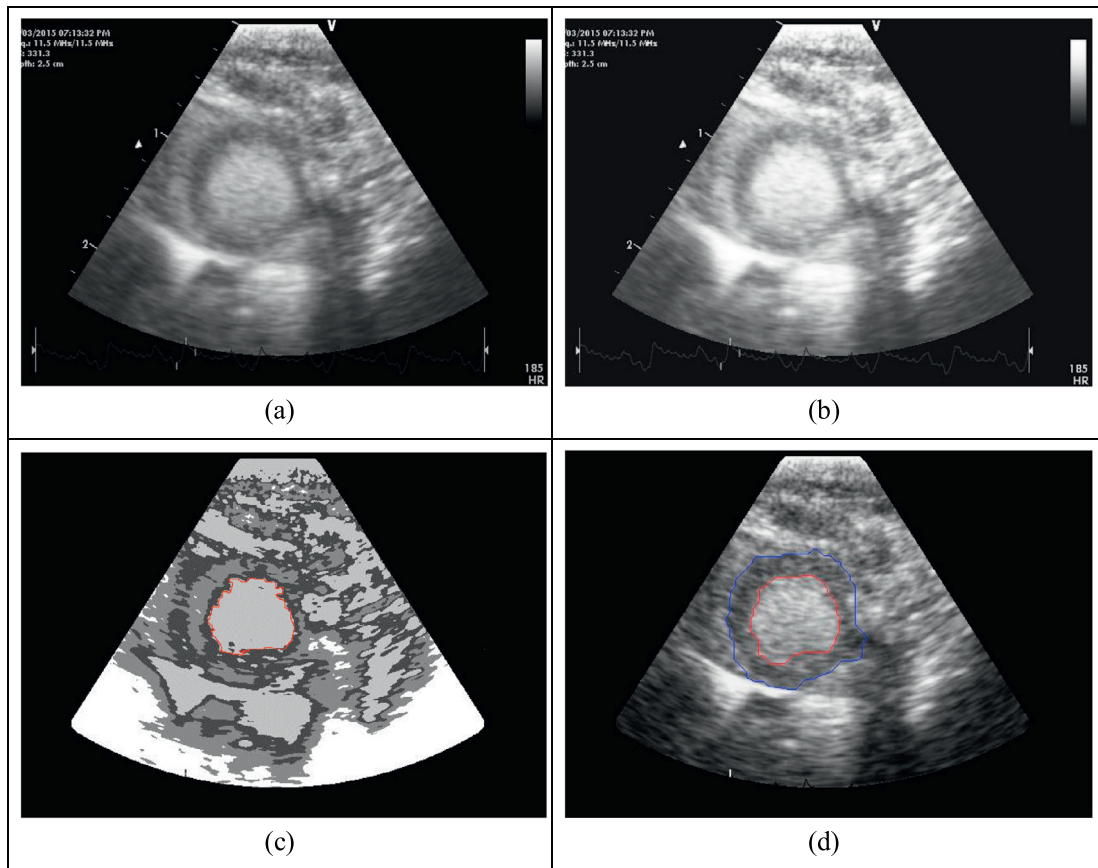


Fig. 1. Results of each step in NACM. (a) Original SLVMCE image. (b) NSV image. (c) Clustering result and initial contour in red line. (d) Myocardium detection result. (For interpretation of the references to color in this figure legend, the reader is referred to the web version of this article.)

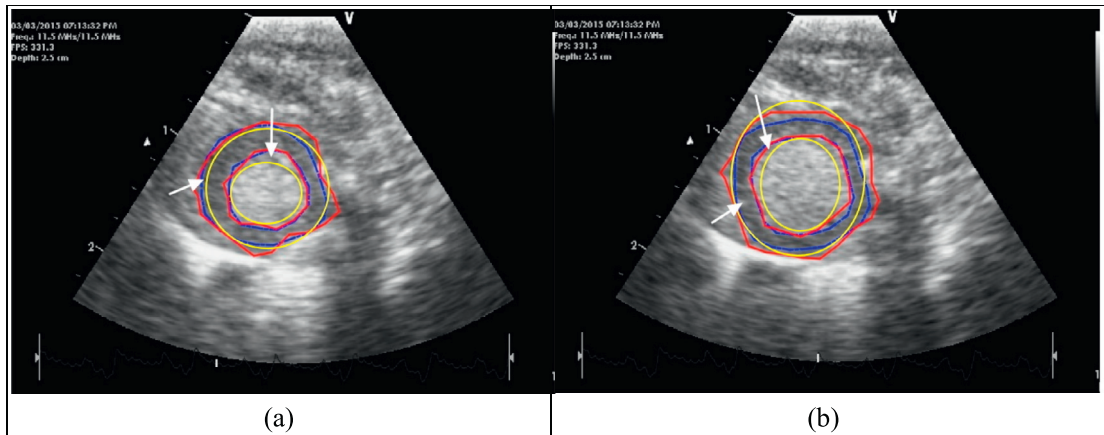


Fig. 2. Comparisons between NACM results and reference standard on one example in different phases. Results by NACM are marked in red, EPSO results by yellow and reference standard by blue. (a) Systole phase (b) Diastole phase. (For interpretation of the references to color in this figure legend, the reader is referred to the web version of this article.)

AvgDist) are calculated on the corresponding images and the mean and standard deviation were computed over all images. Results from the NACM method were also compared with those from the newly published myocardium segmentation algorithm on SLVMCE images using eliminating particle swarm optimization clustering (EPSO) [42]. We also compared the NACM method with a left ventricle segmentation method using active contour model without edges (ACMWE) in ultrasound echocardiographic images [43].

Comparison results are shown in Table 1. The mean and standard deviation of the Hdist and AvgDist on endocardium are decreased from 6.83 ± 1.12 mm, and 0.79 ± 0.28 mm using EPSO

method, and 7.12 ± 0.98 mm, and 0.82 ± 0.32 mm using ACMWE method, to 4.55 ± 0.9 mm, and 0.58 ± 0.18 mm using NACM method, respectively. The improvement on epicardium is much more significant, and two metrics are decreased from 7.45 ± 1.24 mm, and 1.47 ± 0.34 mm using EPSO method, and 8.21 ± 0.43 mm, and 1.73 ± 0.47 mm using ACMWE method, to 4.94 ± 0.82 mm, and 0.84 ± 0.22 mm using NACM method, respectively. The p-values of the differences between the two methods are estimated by the two-tailed Wilcoxon signed rank test. The improvements on four comparisons are statistically significant ($p < 0.05$) for each performance metric according to the p-values. From the

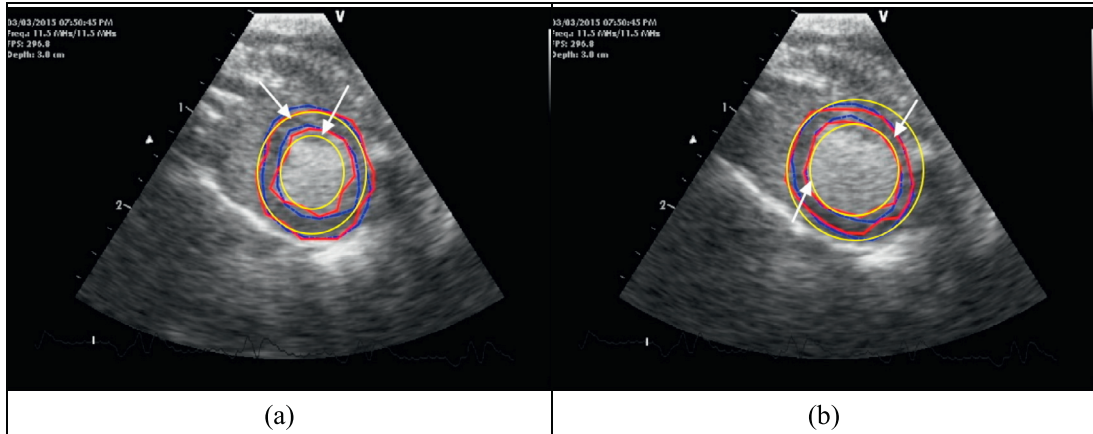


Fig. 3. Comparisons between NACM results and reference standard on one example in different phases. Results by NACM are marked in red, EPSO results by yellow and reference standard by blue. (a) Systole phase (b) Diastole phase. (For interpretation of the references to color in this figure legend, the reader is referred to the web version of this article.)

Table 1
The performance of computer detection results for the EPSO and the NACM methods.

Method	Endocardium		Epicardium	
	Hdist (mm)	AvgDist (mm)	Hdist (mm)	AvgDist (mm)
EPSO	6.83 ± 1.12	0.79 ± 0.28	7.45 ± 1.24	1.47 ± 0.34
ACMWE	7.12 ± 0.98	0.82 ± 0.32	8.21 ± 0.43	1.73 ± 0.47
NACM	4.55 ± 0.9	0.58 ± 0.18	4.94 ± 0.82	0.84 ± 0.22
p-value (EPSO vs NACM)	0.0029	0.028	<10 ⁻¹⁰	<10 ⁻²⁰
p-value (ACMWE vs NACM)	0.0016	0.007	<10 ⁻¹²	<10 ⁻²¹

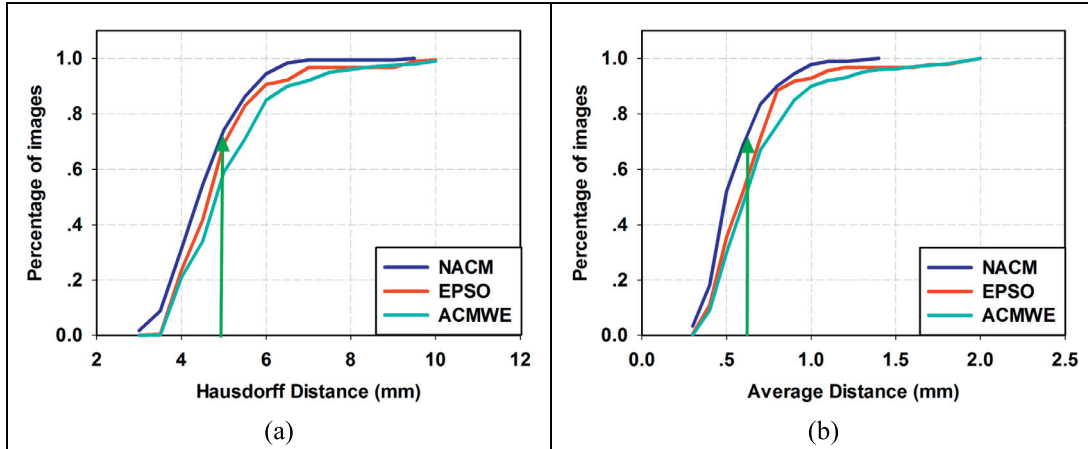


Fig. 4. Cumulative percentage relative to the 182 images with radiologist's manually drawn endocardium as reference standards. (a) Hausdorff distance measure and (b) average Euclidean distance measure between the computer-segmented boundary and the reference standard smaller than a certain value.

comparison results, we can see clearly that the NACM method achieves more accurate segmentation on the myocardium regions in different cases than EPSO and ACMWE methods.

Figs. 4 and 5 show the cumulative percentage of images having Hdist and AvgDist smaller than a certain value on endocardium and epicardium, respectively. In endocardium detection in Fig. 4, for example, 74.2% and 69.2% images in the NACM detected boundaries, 69.2% and 52.5% images in the EPSO detected boundaries, and 59.1% and 48.2% images in the ACMWE detected boundaries, have $Hdist \leq 5$ mm, and $AvgDist \leq 0.6$ mm, respectively. For epicardium results in Fig. 5, for instance, 97.8% and 95.1% cases in the NACM detected boundaries, 31.9% and 24.7% cases in the EPSO detected boundaries, and 30.1% and 25.2% cases in the ACMWE detected boundaries, have $Hdist \leq 7$ mm, and $AvgDist \leq 1.3$ mm, respectively. In the comparison on statistical results, all methods

have better performance on endocardium than that on epicardium due to the endocardium's high contrast and clear boundary with its surround tissue. In addition, the NACM method achieves better detection results than the ACMWE and EPSO methods on both endocardium and epicardium due to employment of a neutrosophic similarity value to deal with the indeterminate information on LSVMCE, and prior knowledge to obtain the initial size of the myocardium as the element size in the dilated operation, which makes the detection result on epicardium more adaptive on different cases with different size and shape of myocardium.

Fig. 6 shows two examples of the under segmentation results. When there is inhomogeneous contrast perfusion in cavity, the ventricle will be not fully enhanced and its boundary is not clear. In this condition, the clustering results of the ventricle region in the proposed method will only identified ventricle region partially

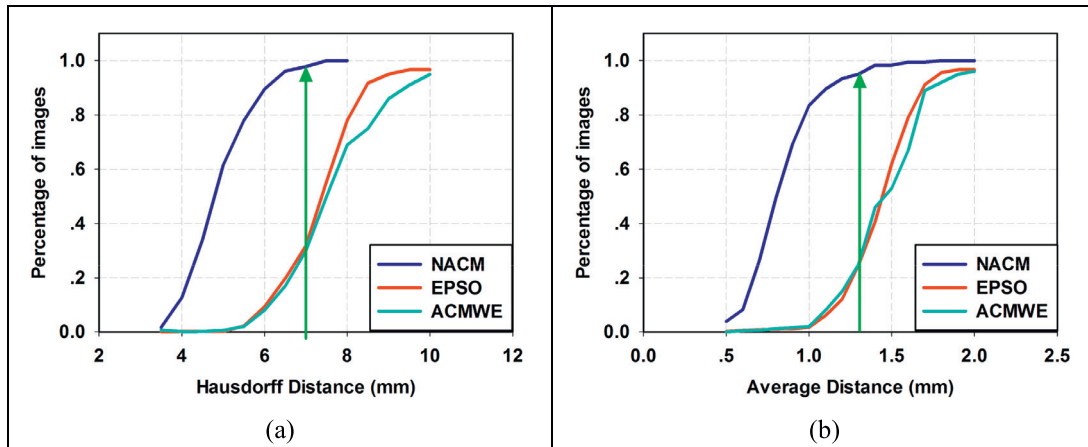


Fig. 5. Cumulative percentage relative to the 182 images with radiologist's manually drawn epicardium as reference standards. (a) Hausdorff distance measure and (b) average Euclidean distance measure between the computer-segmented boundary and the reference standard smaller than a certain value.

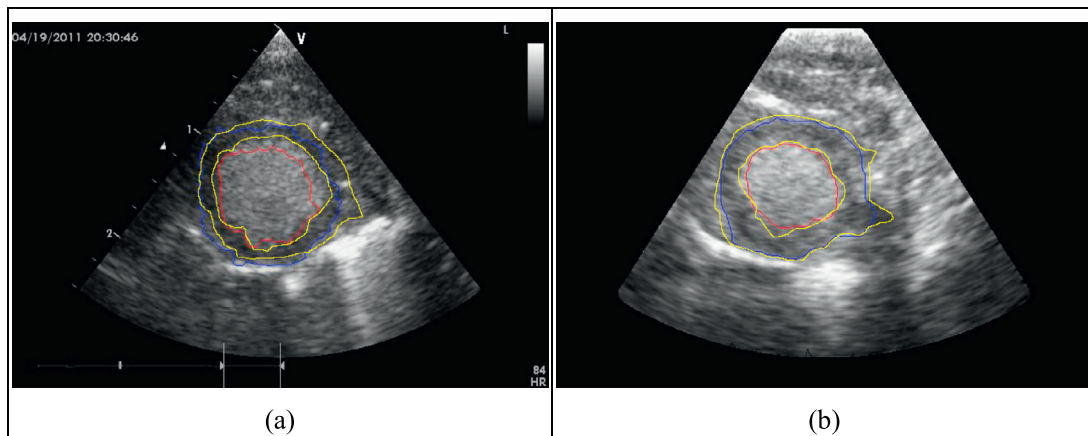


Fig. 6. Examples of under segmentation with references: segmentation boundary in blue and reference boundary in yellow. (For interpretation of the references to color in this figure legend, the reader is referred to the web version of this article.)

which will lead to identify partial boundaries of myocardium and under segmentation of myocardium region. In the future work, we will improve the algorithm to make it robust to the images' quality.

5. Conclusion

In this study, we developed a left ventricular myocardium segmentation algorithm based on neutrosophic similarity score and active contour model. The experimental results demonstrate the proposed NACM method can detect and delineate left ventricular myocardium on contrast echocardiography images quickly and accurately. Future research will introduce automatic measurement of myocardial perfusion, and infarct size in apical long-axis images.

Acknowledgments

This work was supported in part by the National Natural Science Foundation of China (NSFC) (Grant Number: 81371632 and 81671762).

References

- [1] P.Z. Gerczuk, R.A. Kloner, An update on cardioprotection: a review of the latest adjunctive therapies to limit myocardial infarction size in clinical trials, *J. Am. College Cardiol.* 59 (11) (2012) 969–978.
- [2] K. Przyklenk, Reduction of myocardial infarct size with ischemic “conditioning”: physiologic and technical considerations, *Anesthesia Analgesia* 117 (4) (2013) 891–901.
- [3] J.M. Swinburn, A. Lahiri, R. Senior, Intravenous myocardial contrast echocardiography predicts recovery of dysynergic myocardium early after acute myocardial infarction, *J. Am. College Cardiol.* 38 (1) (2001) 19–25.
- [4] S. Téphane Lafitte, A. Higashiyama, H. Masugata, B. Peters, M. Strachan, O.L. Kwan, A.N. DeMaria, Contrast echocardiography can assess risk area and infarct size during coronary occlusion and reperfusion: experimental validation, *J. Am. College Cardiol.* 39 (9) (2002) 1546–1554.
- [5] P. Dourado, J. Tsutsui, W. Mathias Jr, J. Andrade, P. da Luz, A. Chagas, Evaluation of stunned and infarcted canine myocardium by real time myocardial contrast echocardiography, *Brazilian J. Med. Biol. Res.* 36 (11) (2003) 1501–1509.
- [6] A. Yano, H. Ito, K. Iwakura, R. Kimura, K. Tanaka, A. Okamura, S. Kawano, T. Matsuyama, K. Fujii, Myocardial contrast echocardiography with a new calibration method can estimate myocardial viability in patients with myocardial infarction, *J. Am. College Cardiol.* 43 (10) (2004) 1799–1806.
- [7] S. Yamada, K. Komuro, T. Mikami, N. Kudo, H. Onozuka, K. Goto, S. Fujii, K. Yamamoto, A. Kitabatake, Novel quantitative assessment of myocardial perfusion by harmonic power Doppler imaging during myocardial contrast echocardiography, *Heart* 91 (2) (2005) 183–188.
- [8] G. Zwirn, R. Beeri, D. Gilon, S. Akselrod, Automatic endocardial-boundary detection in low mechanical-index contrast echocardiography, *IEEE Trans. Biomed. Eng.* 53 (11) (2006) 2310–2322.
- [9] V. Sudarshan, U.R. Acharya, E.Y.-k. Ng, C.S. Meng, R.S. Tan, and D.N. Ghista, “Automated identification of infarcted myocardium tissue characterization using ultrasound images : a review,” vol. 8, pp. 86–97, 2015.
- [10] W. Zhang, J.A. Noble, J.M. Brady, Real time 3-D ultrasound to MR cardiovascular image registration using a phase-based approach, in: 3rd IEEE International Symposium on Biomedical Imaging: Nano to Macro, 2006, 2006, pp. 666–669.
- [11] R. Sigit, M.M. Mustafa, A. Hussain, O. Maskon, I.F.M. Nor, On the use of collinear and triangle equation for automatic segmentation and boundary detection of cardiac cavity images, in: Software Tools and Algorithms for Biological Systems, Springer, 2011, pp. 481–488.
- [12] C.H. Seng, R. Demirli, M.G. Amin, J.L. Sechrist, A. Bouzerdoum, Automatic left ventricle detection in echocardiographic images for deformable contour initialization, in: Engineering in Medicine and Biology Society, EMBC, 2011 Annual International Conference of the IEEE, 2011, pp. 7215–7218.

- [13] N. Technologies, "Left ventricular segmentation of 2-D echocardiographic image : a survey," pp. 563–566, 2011.
- [14] T. Dietenbeck, D. Barbosa, M. Alessandrini, R. Jasaitytė, V. Robesyn, J. D'hooge, D. Friboulet, O. Bernard, Whole myocardium tracking in 2D-echocardiography in multiple orientations using a motion constrained level-set, *Med. Image Anal.* 18 (3) (2014) 500–514.
- [15] T. Dietenbeck, M. Alessandrini, D. Barbosa, J. D'hooge, D. Friboulet, and O. Bernard, "Detection of the whole myocardium in 2D-echocardiography for multiple orientations using a geometrically constrained level-set," *Med. Image Anal.*, vol. 16, no. 2, pp. 386–401.
- [16] M. Lynch, O. Ghita, P.F. Whelan, Left-ventricle myocardium segmentation using a coupled level-set with a priori knowledge, *Comput. Med. Imag. Graph.* 30 (4) (2006) 255–262.
- [17] A.L.N. Wong, H. Liu, P. Shi, Segmentation of myocardium using velocity field constrained front propagation, in: *Applications of Computer Vision, 2002. (WACV 2002). Proceedings. Sixth IEEE Workshop on, 2002*, pp. 84–89.
- [18] C. Li, X. Jia, Y. Sun, Improved semi-automated segmentation of cardiac CT and MR images, in: *Biomedical Imaging: From Nano to Macro, 2009. ISBI '09. IEEE International Symposium on*, Boston, MA, 2009, pp. 25–28.
- [19] M. Lynch, O. Ghita, and P.F. Whelan, "Automatic segmentation of the left ventricle cavity and myocardium in MRI data," vol. 36, pp. 389–407, 2006.
- [20] L. Cordero-grande, G. Vegas-sánchez-ferrero, P. Casaseca-de-la-higuera, Unsupervised 4D myocardium segmentation with a Markov random field based deformable model, *Med. Image Anal.* 15 (3) (2011) 283–301.
- [21] V. Lempitsky, M. Verhoeck, J.A. Noble, A. Blake, Random forest classification for automatic delineation of myocardium in real-time 3D echocardiography, *Functional Imag. Model. Heart, The Series Lecture Notes in Computer Science* 5528 (2009) 447–456.
- [22] Y. Li, C.P. Ho, N. Chahal, R. Senior, M.-X. Tang, Myocardial segmentation of contrast echocardiograms using random forests guided by shape model, in: S. Ourselin, L. Joskowicz, M.R. Sabuncu, G. Unal, W. Wells (Eds.), *Medical Image Computing and Computer-Assisted Intervention – MICCAI 2016: 19th International Conference, Athens, Greece, October 17–21, 2016, Proceedings, Part III*, Cham: Springer International Publishing, 2016, pp. 158–165.
- [23] V. Lempitsky, M. Verhoeck, J.A. Noble, A. Blake, Random forest classification for automatic delineation of myocardium in real-time 3d echocardiography, in: *Proceedings of the 5th International Conference on Functional Imaging and Modeling of the Heart, Nice, France, 2009*, pp. 447–456.
- [24] Y. Guo, H.-D. Cheng, New neutrosophic approach to image segmentation, *Pattern Recogn.* 42 (5) (2009) 587–595.
- [25] A. Sengur, Y. Guo, Color texture image segmentation based on neutrosophic set and wavelet transformation, *Comput. Vis. Image Understand.* 115 (8) (2011) 1134–1144.
- [26] Y. Guo, A. Sengür, A novel image segmentation algorithm based on neutrosophic filtering and level set, *Neutrosophic Sets Syst.* 46 (2013).
- [27] E. Karabatak, Y. Guo, A. Sengur, Modified neutrosophic approach to color image segmentation, *J. Electron. Imag.* 22 (1) (2013) 013005–013005.
- [28] B. Yu, Z. Niu, L. Wang, Mean shift based clustering of neutrosophic domain for unsupervised constructions detection, *Optik-Int. J. Light Electron Optics* 124 (21) (2013) 4697–4706.
- [29] K.I. Laws, Textured image segmentation, DTIC Document (1980).
- [30] M. Kass, A. Witkin, D. Terzopoulos, Snakes: active contour models, *Int. J. Comput. Vis.* 1 (4) (1988) 321–331.
- [31] Y. Guo, A. Sengur, A novel color image segmentation approach based on neutrosophic set and modified fuzzy c-means, *Circuits Syst. Signal Process.* 32 (4) (2013) 1699–1723.
- [32] Y. Guo, A. Şengür, A novel image segmentation algorithm based on neutrosophic similarity clustering, *Appl. Soft Comput.* 25 (2014) 391–398.
- [33] Y. Guo, A. Şengür, J. Ye, A novel image thresholding algorithm based on neutrosophic similarity score, *Measurement* 58 (2014) 175–186.
- [34] Y. Guo, A. Sengur, NCM: neutrosophic c-means clustering algorithm, *Pattern Recogn.* 48 (8) (2015) 2710–2724.
- [35] Y. Guo, R. Xia, A. Şengür, K. Polat, A novel image segmentation approach based on neutrosophic c-means clustering and indeterminacy filtering, *Neural Comput. Appl.* (2016) 1–11.
- [36] J.R. Lindner, J. Sklenar, Placing faith in numbers: quantification of perfusion with myocardial contrast echocardiography*, *J. Am. College Cardiol.* 43 (10) (2004) 1814–1816.
- [37] P.A. Dijkmans, R. Senior, H. Becher, T.R. Porter, K. Wei, C.A. Visser, O. Kamp, Myocardial contrast echocardiography evolving as a clinically feasible technique for accurate, rapid, and safe assessment of myocardial perfusion: the evidence so far, *J. Am. College Cardiol.* 48 (11) (2006) 2168–2177.
- [38] F. Pathan, T.H. Marwick, Myocardial perfusion imaging using contrast echocardiography, *Progress Cardiovascular Dis.* 57 (6) (2015) 632–643.
- [39] B.N. Shah, N.S. Chahal, S. Bhattacharyya, W. Li, I. Roussin, R.S. Khattar, R. Senior, The feasibility and clinical utility of myocardial contrast echocardiography in clinical practice: results from the incorporation of myocardial perfusion assessment into clinical testing with stress echocardiography study, *J. Am. Soc. Echocardiograph.* 27 (5) (2014) 520–530.
- [40] M. Jacobs, M. Benovoy, L.-C. Chang, A.E. Arai, L.-Y. Hsu, Evaluation of an automated method for arterial input function detection for first-pass myocardial perfusion cardiovascular magnetic resonance, *J. Cardiovascular Magnetic Reson.* 18 (1) (2016) 17.
- [41] P.J. Slomka, H. Nishina, D.S. Berman, X. Kang, J.D. Friedman, S.W. Hayes, U.E. Al-Adl, G. Germano, Automatic quantification of myocardial perfusion stress–rest change: a new measure of ischemia, *J. Nuclear Med.* 45 (2) (2004) 183–191 1, 2004.
- [42] G.-Q. Du, J.-Y. Xue, Y. Guo, S. Chen, P. Du, Y. Wu, Y.-H. Wang, L.-Q. Zong, J.-W. Tian, Measurement of myocardial perfusion and infarction size using computer-aided diagnosis system for myocardial contrast echocardiography, *Ultrasound Med. Biol.* 41 (9) (2015) 2466–2477.
- [43] A. Skalski, P. Turcza, T. Zieliński, J. Królczyk, T. Grodzicki, Left ventricle USG image segmentation using active contour model, *Procedia Comput. Sci.* 1 (1) (2010) 2723–2732.